

---

# DEVELOPMENT OF A MODULAR AND SUBMERSIBLE SOFT ROBOTIC ARM AND CORRESPONDING LEARNED KINEMATICS MODELS <sup>\*†‡§</sup>

---

**W. David Null**

Department of Electrical and Computer Engineering  
University of Illinois Urbana-Champaign  
Urbana, IL  
null2@illinois.edu

**Y Z**

Department of Nuclear Engineering and Radiological Sciences  
University of Michigan  
Ann Arbor, MI  
yzyz@umich.edu

## ABSTRACT

Most soft-body organisms found in nature exist in underwater environments. It is helpful to study the motion and control of soft robots underwater as well. However, a readily available underwater soft robotic system is not available for researchers to use because they are difficult to design, fabricate, and waterproof. Furthermore, submersible robots usually do not have configurable components because of the need for sealed electronics packages. This work presents the development of a submersible soft robotic arm driven by hydraulic actuators which consists of mostly 3D printable parts which can be assembled in a short amount of time. Also, its modular design enables multiple shape configurations and easy swapping of soft actuators. As a first step to exploring machine learning control algorithms on this system, two deep neural network models were developed, trained, and evaluated to estimate the robot's forward and inverse kinematics. The techniques developed for controlling this underwater soft robotic arm can help advance understanding on how to control soft robotic systems in general.

**Keywords** Soft Robotics · Control Systems · Neural Networks · Underwater Robotics · Hydraulic Actuator

## 1 Introduction

Despite excellent performance in organized and repeatable manual tasks, traditional robotic systems are incapable of realizing their full potential due to their inability to operate effectively in unknown or changing environments or near humans [1, 2]. Human expertise in operating in dynamic environments comes in part from the advantages of compliance provided in human skin and muscles. Robots must be able to achieve synchronization between rigid and soft components to receive the complementary benefits of both. While there are many active research areas exploring soft robots, this work is primarily concerned with understanding the motion and control of soft hydraulic actuators [3] which have promising applications in minimally invasive surgery (MIS) [4], underwater remotely operated vehicles (UROVs) [5], and biomimicry [6].

---

<sup>\*</sup>Department of Electrical and Computer Engineering, University of Illinois at Urbana-Champaign, Urbana, IL 61801, USA

<sup>†</sup>Beckman Institute for Advanced Science and Technology, University of Illinois at Urbana-Champaign, Urbana, IL 61801, USA

<sup>‡</sup>Department of Nuclear, Plasma, and Radiological Engineering, University of Illinois at Urbana-Champaign, Urbana, IL 61801, USA

<sup>§</sup>Department of Nuclear Engineering and Radiological Sciences, University of Michigan, Ann Arbor, MI 48109, USA

The most successful organisms made from mostly soft materials exist underwater. As a result, there have been many studies on methods of locomotion in underwater environments inspired by biological design [6, 7, 8, 9, 10, 11, 12]. Some of these inspired soft robotic designs have exciting practical applications such as exploring the Mariana Trench [13] or silently hovering over the ocean floor [14]. Because soft actuators are severely under-actuated, it is challenging for them to oppose external forces such as gravity, friction, and disturbances. Water acts as a passive actuator by counteracting the force of gravity, reducing the friction coefficient for many surfaces, and dampening any oscillations that may occur because of an external impact on the robot.

Soft hydraulic actuators are fitting for use in underwater environments because the source of fluid is readily abundant. Researchers have exploited this advantage by implementing several underwater soft robotic arms and manipulators [5, 15, 16, 17, 18, 19, 20, 21]. Miniaturized versions of these robots have potential use cases in MIS [4] where the robot can be surrounded by blood [22]. Furthermore, insights on the characteristics of underwater soft robots can also be applied more generally as Du et al. showed by improving a simulation model developed for an underwater robot [23].

Hydraulically actuated underwater soft robots have immense potential, however, designing accurate and robust controllers for these systems remains a challenge despite their natural advantages. High nonlinearity and large degrees of freedom render analytical models, such as piecewise constant curvature (PCC) [24], insufficient. The finite element method has been applied successfully to simulate soft robots [25] but suffers from large computational complexity which limits its usability on real time systems [26]. In traditional controller design, feedback techniques are used to compensate for modelling errors. However, despite exciting new developments in soft sensors research [27, 28], the sensors themselves are not readily available, and are difficult to fabricate, install, and calibrate.

At this point, researchers have turned to data driven modelling and control strategies to capture the nuances of a system's nonlinearity, while running in real time [29]. A widely used method is learning the forward and inverse kinematics of a soft robot with a neural network [30]. Deep neural networks and recursive neural networks have also been used to develop a model for use in a model predictive controller [31, 32, 33]. A problem with these approaches is that a disturbance or change to the robot's weight can cause the estimated models to break down for lack of sufficient data. Thus, reinforcement learning has been proposed as a model-free approach to the problem [29, 34]. A method based on Gaussian Process Regression can update its policies online to account for disturbances [35].

This work presents the development of a submersible soft robotic arm with a modular design which is simple to assemble, and useful for research. The mechanical structure consists of 3D printed parts, and the actuator molds can also be 3D printed. It can collect internal state data from pressure sensors and solenoids positioned locally to each actuator and synchronize this with ground truth positioning information gathered from an overhead camera. Its design is such that its soft hydraulic actuators can be easily swapped with those of different shapes, sizes, and material characteristics. Additionally, it consists of individual segments whose electronics and fluid networks can attach to each other. These segments can be added and subtracted to reach a desired robot configuration. This work also presents the development of two learned kinematic models. The first can predict the shape of the robot given a set of internal state variables and the second can compute the internal pressure values for the hydraulic actuators given a valid robot shape.

## 2 Materials and Methods

### 2.1 Experimental Setup

The entire system was built to work in a desktop configuration for rapid algorithm development and testing. In the desktop configuration, the robot's base plate is mounted to a sheet of acrylic and submerged in about 5 cm of water along with the water pump which creates the hydraulic pressure as seen in (Figure 1(d)). The tank itself is a plastic storage container about two feet wide and four feet long. Arrayed along the middle of the robot are computer vision (CV) markers shown in (Figure 1(a)) which are used to track the true shape of the robot. The water level is such that the CV markers rest just above the surface so they can easily be seen by the camera positioned directly above the robot as shown in (Figure 1). Computer vision was used over motion capture because of infrared reflectance off the water's surface and the camera can be calibrated to operate underwater if needed. The camera and the robot are both controlled by the main computer which is a Raspberry Pi 4 for this project.

The robot presented has two similar modules stacked on top of each other. Both modules consist of two soft actuators, and each is driven by 2 solenoid valves and sensed by one pressure sensor. The actuators are fabricated out of a silicon using 3D printed molds shown in (Figure 2). A DC pump creates the pressure which is channeled through the network of tubes and valves shown in (Figure 2). On each module's local PCB, there are two pressure sensors which puts them very close to the actuators themselves shown in (Figure 1) and (Figure 1). This ensures a more accurate reading. The camera is positioned directly above the robot and can be seen in (Figure 1). The samples from the pressure sensors are synchronized with photos taken from the camera.

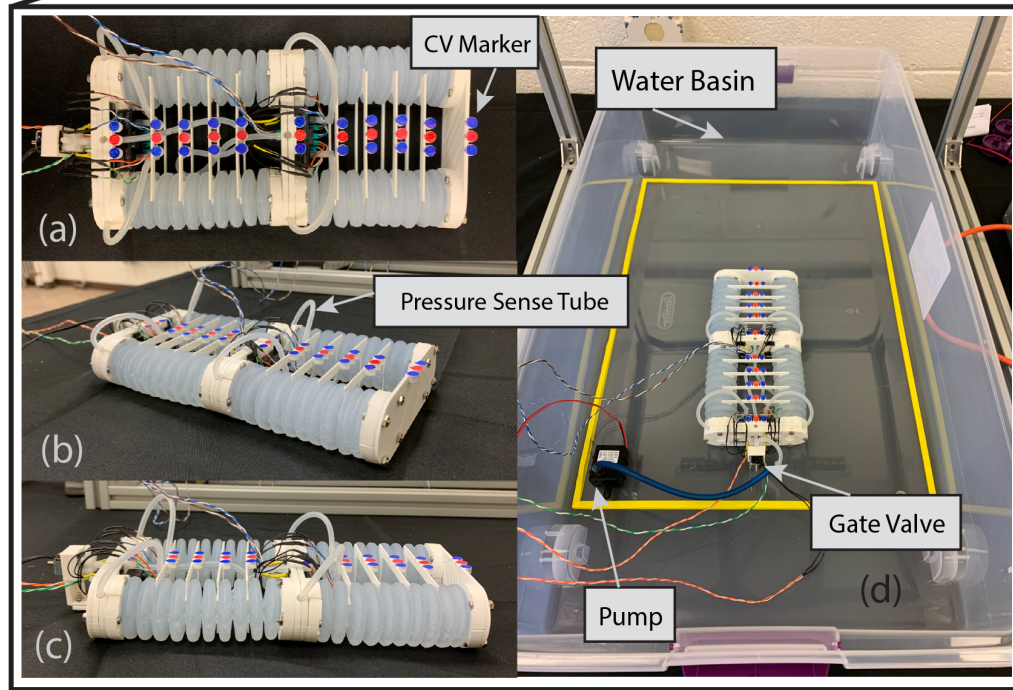
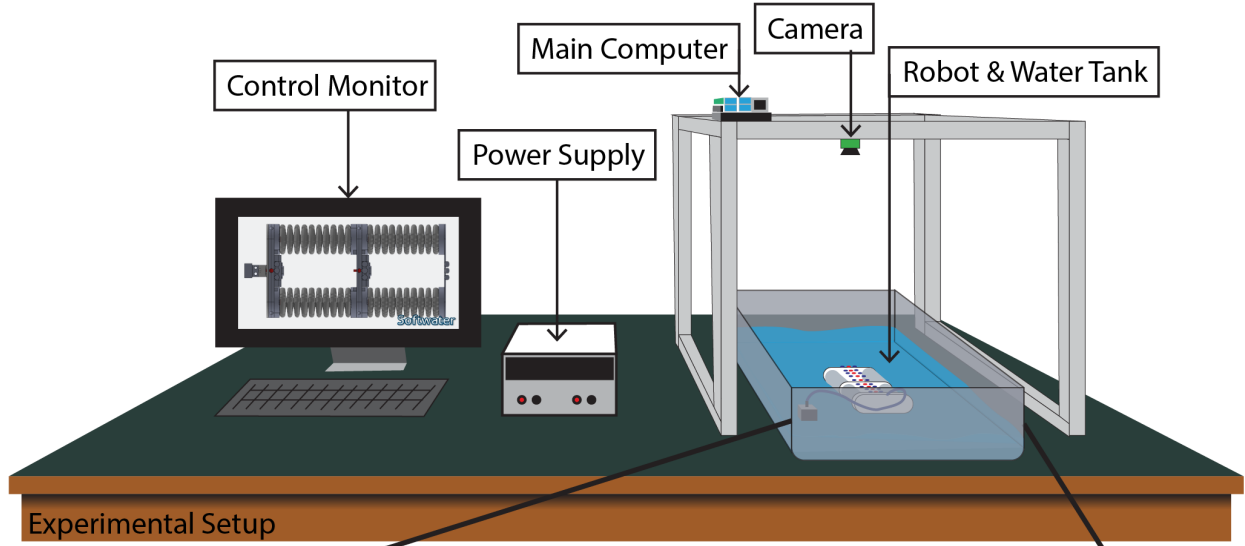


Figure 1: Desktop configuration of the robot and (a) Top view of robot with computer vision markers shown. (b) Isometric view of robot with pressure sensor tubes shown. (c) Side view of robot. (d) Bird's eye view of robot in empty water basin with pump and gate valve shown.

## 2.2 Modular Design

One of the key features of this soft robotic system is its modular design. The electronic, mechanical, and hydraulic components are all built so that modules can be stacked on top of each other to form different configurations for different experiments and applications. These can be seen in (Figure 2), and (Figure 3) and (Figure 4). Similarly, the actuators themselves can be swapped out easily. This enables easier maintenance as well as different shapes, sizes, and material properties to be tested on the same system. The system's modularity creates potential for many different research applications.

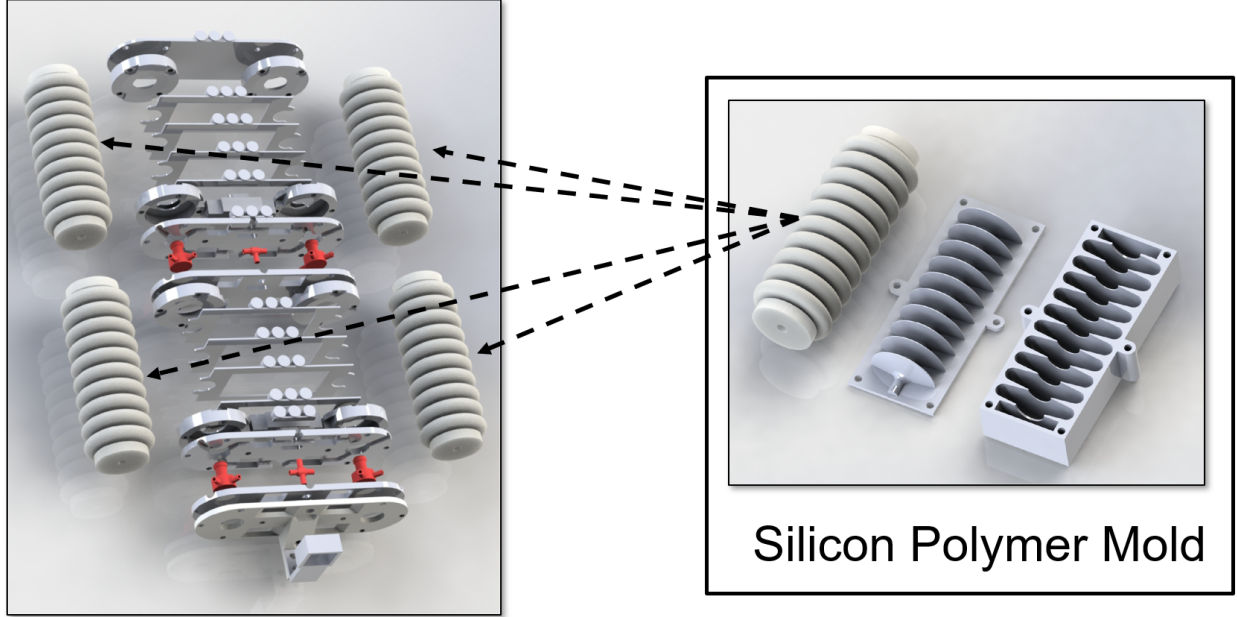


Figure 2: Exploded view of the soft robotic system and render of actuator and 3D printed mold used for fabrication.

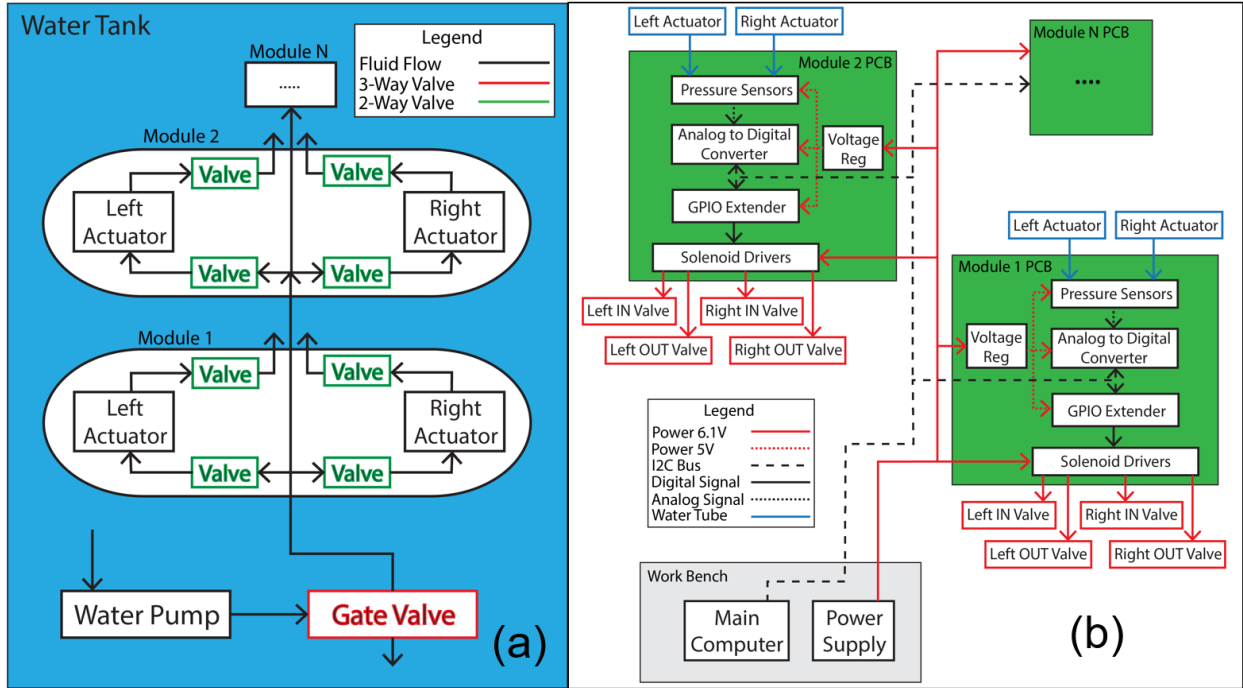


Figure 3: Block diagrams of design demonstrating modularity for the (a) hydraulic systems and (b) electronic systems.

### 2.3 Mathematical Representation of Robot

Before developing the model, it is necessary to first represent the robot in mathematical terms as demonstrated in (Figure 5). As shown the robot is constructed of two modules with module one being the base module which is fixed in space. Each module has five CV markers labelled  $m_{i,j}$  where  $i \in \{1, 2\}$  and  $j \in \{1, 2, 3, 4, 5\}$  and the base CV marker which is fixed in space  $m_{0,0}$  represents the origin. Each CV marker contains three circles whose centroid locations can be identified by a camera located above the robot. The red circle in the middle represents the center of that section of



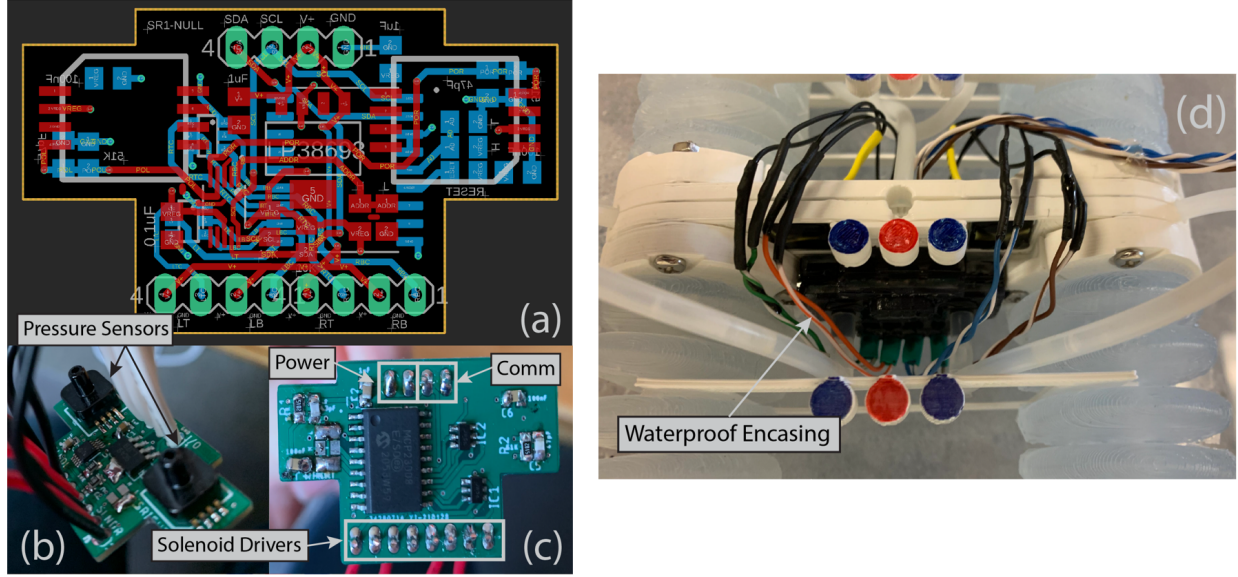


Figure 4: (a) Board design (b) Top of the board showing pressure sensors (c) Bottom of board showing solenoid driver outputs, power, and I2C communication connections (d) Board in waterproof enclosure installed on robot.

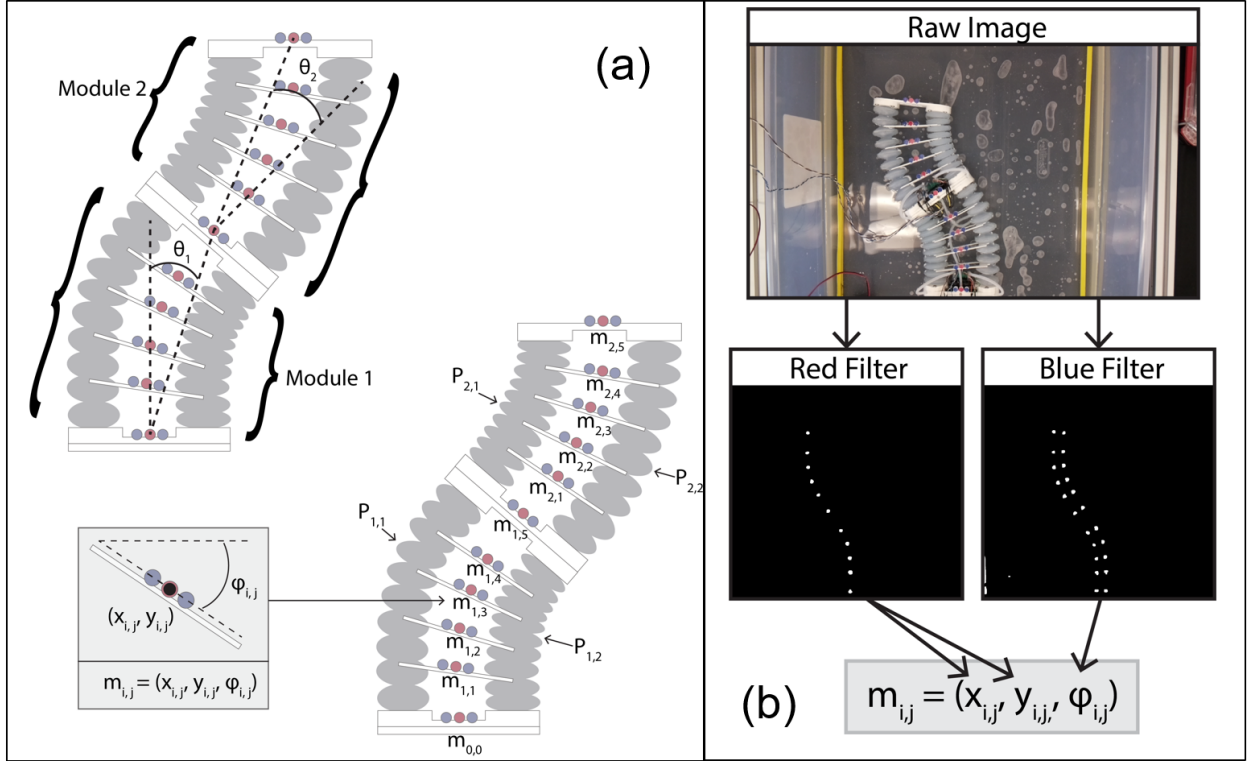


Figure 5: (a) Mathematical representation of robotic system. (b) Filter outputs generated from raw image to reveal locations of CV markers.

the robot and is given an  $(x, y)$  location. All the red circles together represent the underlying shape configuration of the robot. The blue markers make it possible to draw a line parallel to the middle support structure which yields the orientation of that section of the robot with respect to the horizontal. This orientation is represented by an angle  $\phi$  as

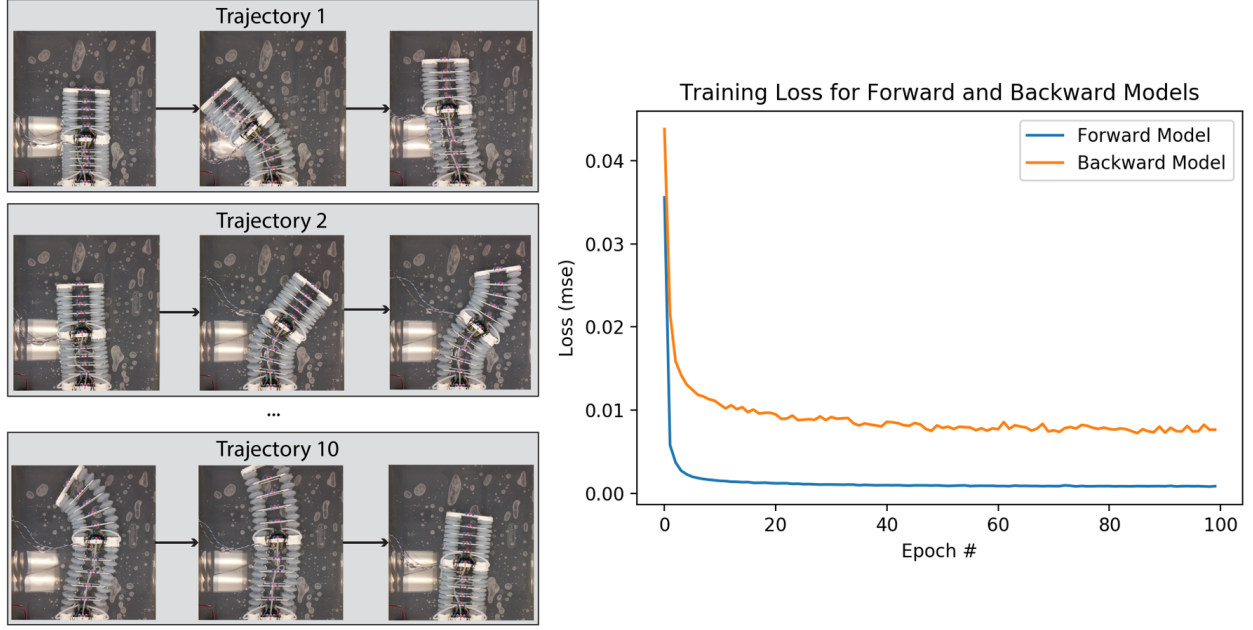


Figure 6: Examples of partial trajectories used to generate training data for neural networks and Training loss for both models as a function of each epoch.

shown in (Figure 5). All this information is captured in one marker tuple as  $m_{i,j} = (x_{i,j}, y_{i,j}, \phi_{i,j})$ . The pressure value for each actuator is denoted by the symbol  $P_{a,b}$  where  $a \in \{1, 2\}$  for modules 1 and 2 and  $b \in \{1, 2\}$  for left and right.

## 2.4 Data Collection

To generate raw data for training, the robot was actuated along 10 different trajectories which brought each actuator to its limit in different configurations with other actuators. Examples from parts of these trajectories are shown in (Figure 6). Each one lasted between 8-17 minutes and were designed to reach the limits of the robot's configuration space, however, one limitation placed on them was that only one actuator could be pressurized or depressurized at a time. The data collected at each time step with a frequency of 2 Hz consisted of the four pressure values from each actuator, the eight in/out solenoid valve states, the state of the pump (on/off), the state of the gate valve, and a 1080p image of the robot.

After the raw data was collected, the images were analyzed to extract the positions of the red circle centroids to describe the shape of the robot. The outputs of the computer vision filters are shown in (Figure 5). To create these filters, the images were first converted to HSV format, then blurred using a Gaussian blur with a kernel size of 25, then filtered using bounding thresholds found to work for the red and the blue colors. Finally, the outputs within the thresholds were eroded and dilated to refine their shapes and finally the minimum enclosing circle found the radius and the center of each blob representing the markers on the robot. These operations were executed using the open-source software package, OpenCV. The positions of each marker were appended to the main data set for the times corresponding to when the image was taken.

Finally, all the data was normalized in preparation for use in a neural network. The normalization thresholds were chosen to preserve the relative differences between pressure values and x and y values of markers. All pressure values were normalized between 95 kPa and 121 kPa, all x marker values between -15 cm and 15 cm, and all y marker values between 0 cm and 40 cm. With the data normalized, it was ready to be passed to a neural network for training.

## 2.5 Neural Network and Model Structures

Using the data collected, two deep neural networks (DNN) were designed, trained, and tested to model the forward and inverse kinematics of submersible soft robotic system. These DNNs are referred to as the forward and the backward model. The forward model takes in robot state parameters and outputs estimated CV marker positions for all 10 markers. On the other hand, the backward model takes as input the ground truth marker locations for a single time step and outputs the pressure values which are characteristic of that specific shape.

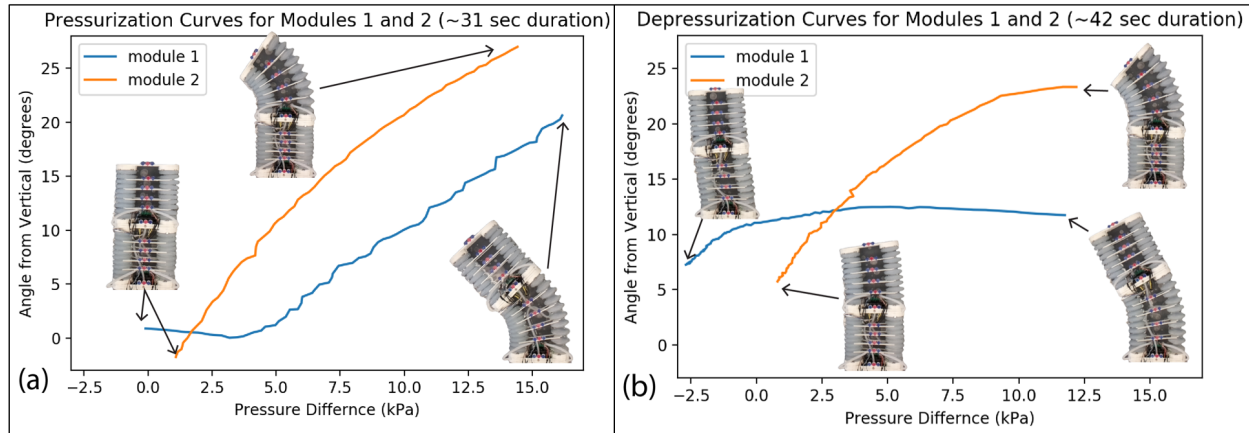


Figure 7: Robot characterization data plots angle from vertical ( $\theta_1$ , and  $\theta_2$ ) vs. pressure difference between right and left actuator for module 1 and 2.

There are a few sets of robot state parameters which are inputs to the forward network. The intrinsic parameters which are most related to the shape of the robot are the pressures in each actuator and the state of the in/out solenoid valves. The valves reveal whether an actuator is being pressurized or depressurized which can lead to a different interpretation of the pressure data. Also, because the motion of the robot is highly dependent on its previous states as shown in (Figure 7), previous slices of robot state data for the pressure values and the in/out valves are also fed as inputs to the forward model. In total there are slices of state data from four time-steps starting at the most recent and jumping backward seven time-steps or (3.5 seconds) at a time. The output of this neural network are the x and y positions of the ten CV markers which are labelled with ground truth data from the images recorded. This network is useful for predicting the shape of the robot given current state data.

The backward network is much simpler. Its inputs are simply the desired true x and y positions of the 10 CV markers down the middle of the robot, and the outputs are the 4 pressure values of each actuator. This network would be useful in determining pressure values to reach to get the robot to a certain position or shape.

Both networks were built using Keras. Having a similar internal structure, they consist of 4 dense hidden layers each of which uses a relu activation function and is followed by a dropout layer with a probability value of 0.2. The dense layers have a size of 128, 64, 32, and 16 neurons respectively. The difference between the forward and the backward model are the input and output dimensions. In total, the forward network has 17,476 trainable parameters while the backward network has 13,620 trainable parameters. Both networks are trained using mean squared error as the loss function and the “adam” optimizer.

### 3 Results

#### 3.1 Basic Actuation Experiment

By examining the pressurization and depressurization curves of an actuator in the top vs bottom modules, we observe some of the nonlinear characteristics of the system which need to be learned. Annotated experimental data is shown in (Figure 7). The data is meant to show the angular displacement of each module as a function of the pressure difference between its two actuators. For both graphs, the x-axis is the pressure difference between the left and right actuators for that module calculated by the equation  $P_{\text{diff}} = P_{i,2} - P_{i,1}$  where  $i \in \{1, 2\}$  for modules 1 and 2. The y-axis is the angle from vertical for each module corresponding to the values for  $\theta_1$  and  $\theta_2$  shown in (Figure 5). The data in (Figure 7(a)) was taken over the course of about 31 seconds (viewed from left to right on the plot) as the right actuator for each module was being pressurized. Whereas the data in (Figure 7(b)) was taken over the course of about 41 seconds (viewed from right to left on the plot) as the right actuator for each module was being depressurized.

These plots give us insights into the movements of the robot. First, pressurization takes less time than depressurization for both modules. This makes sense as during pressurization, the flow of water into the actuator is mostly constant and driven by the pump. However, during depressurization, the force expelling water from the actuators is driven by the actuator itself trying to get back to equilibrium. As with the force of a spring, this force is not constant and decreases as the actuator shrinks. This also leads to the different shapes for the pressurization and depressurization curves. Secondly, module 1 demonstrates more severe hysteresis than module 2. This is evidenced by the fact that

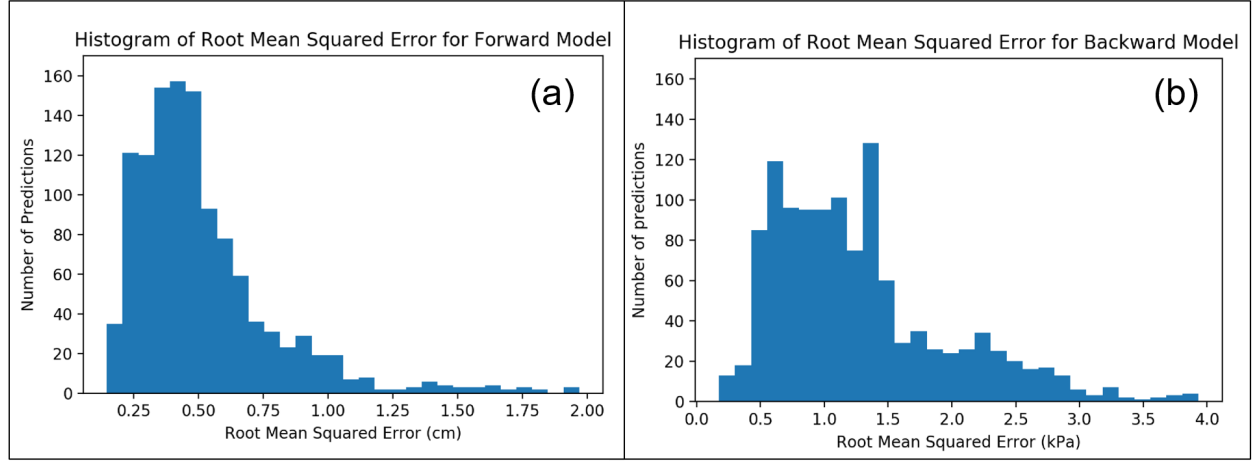


Figure 8: Histogram of root mean squared error (RMSE) over the testing data set for the forward model (top) and the backward data set (bottom).

the angular displacement for module 1 does not start increasing during pressurization until the pressure difference is nearly 3.7 kPa. Whereas the angular displacement starts increasing for module 2 almost immediately when the pressure difference starts increasing. A similar trend is also seen in the depressurization curves. This is explainable because module 1 needs to drag along module 2 wherever it goes and therefore requires more force to start moving. Finally, it is interesting that the pressure difference goes negative at the end of depressurization for module 1 shown in (Figure 7(b)). This means that the pressure for the left actuator is greater than the pressure in the right actuator by 2.5 kPa even though no water entered the left actuator during this time. This happens because as the right actuator shrinks, it causes the right actuator to compress as well causing the increase in pressure because its out-valve is closed. All these characteristics of the system are extremely difficult to model analytically with sufficient accuracy. However, it is possible to learn these dynamics as shown in the next sections.

### 3.2 Model Training

The data used for training and testing the networks was taken from the 10 tracked trajectories discussed earlier. In total, there were 5,886 data points which were shuffled and split 80%/20% for training and testing respectively. Both models were trained over 100 epochs with a batch size of 8. The training loss curves for both networks are shown in (Figure 6). The forward model performs better in training than the backward model. Both models do not suffer from over-fitting as shown by their average loss when evaluated on the testing data being less than their final losses achieved on the training data.

### 3.3 Model Performance

(Figure 8) shows the histograms of the root mean squared errors (RMSE) when evaluating both models on the same testing data points. The forward model performs very well with most of the shape estimations averaging less than 5 millimeters of error per CV marker position. The errors for the backward model are more spread out over a range of errors. This again shows the forward model outperforming the backward model.

The first model is called the “forward” model because it estimates the robot’s forward kinematics. Given a set of internal robot parameters over a series of 4 time-steps including the current time-step, it estimates the output of the robot’s shape. This type of model is useful in computing a robot’s horizon in a model predictive controller or generating training trajectories in a reinforcement learning algorithm. This model performs very well overall. When evaluated on the test set of 1,178 data points, about 60% of the estimated robot shapes returned less than 5mm average error from the actual robot shapes. The worst performing shape estimates, which only had about 1.5 cm average error occurred when the robot was at its limits of operation as in (Figure 9(a,b)), or when there was prolonged steady state error (Figure 9(c)). This steady state error occurred because the actuators in the first module are not able to drag the second module all the way back to the centered home position. Thus, the pressure is equalized for an extended period, but the position of the robot is not where it normally would be. It would be interesting to see if fabricating the actuators on the first module with a stiffer material would solve this issue.



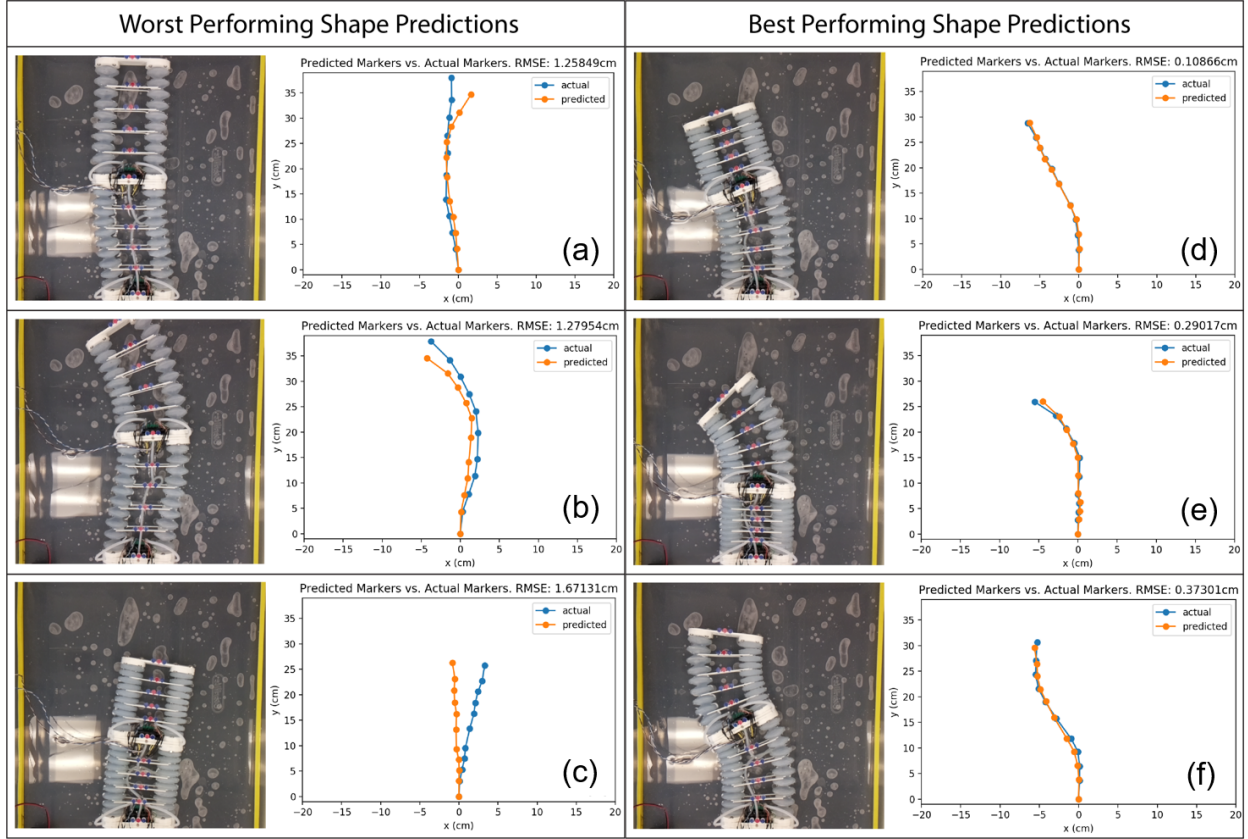


Figure 9: (a-c) Poor performing estimated shape configurations generated by forward model. (d-f) Good performing estimated shape configurations generated by the forward model.

The second model is called the “backward” model because it estimates the robot’s inverse kinematics. Given as input the robot’s shape, it estimates the pressure values in each actuator. This model is useful for generating final pressure values to reach a target location. It can also be used to generate a trajectory of pressures to reach a target location while avoiding obstacles. While it did not perform as well as the forward model, as shown by its error histogram in (Figure 8), it was also given much less information as an input. The reason for this is that it is not always possible to track the shape of the robot over time. Often the robot arm will be operating in a space where a camera cannot see its full shape. Thus, only the target shape and the robot’s current state is known. Even with these minimal input parameters, the model performs good enough for some applications. Some pressure values corresponding to some complex shapes were predicted successfully with 1.4 kPa of average error between the pressure values as seen in (Figure 9).

Visual representations of the performance of the two models are shown the following examples. Figure (Figure 9(a,b,c)) shows some of the worst performing shape predictions of the forward model. Two of these occur when both modules are extended near their limit, and one occurs near the robot’s home position where both modules are fully depressurized. This last one shows steady state error caused typically because module 1 is not strong enough to fully drag module 2 back home but the pressure appears as if both modules are completely depressurized. Figure (Figure 9(d,e,f)) shows some of the best performing shape estimations made from the forward model. Likewise, Figure (Figure 10(a,b,c)) shows some of the worst performing pressure predictions from the backward model and Figure (Figure 10(d,e,f)) shows some of the best.

## 4 Discussion and Conclusion

Advancements in the field of soft robotics represent steps toward robots realizing their full potential. When we look to nature to help us understand soft robotics, we find that the most successful organisms whose bodies are made primarily from soft materials exist in underwater environments. This has evoked much interest in studying submersible soft robots. This work presents an underwater soft robotic arm that is not only relatively simple to assemble but also modular and



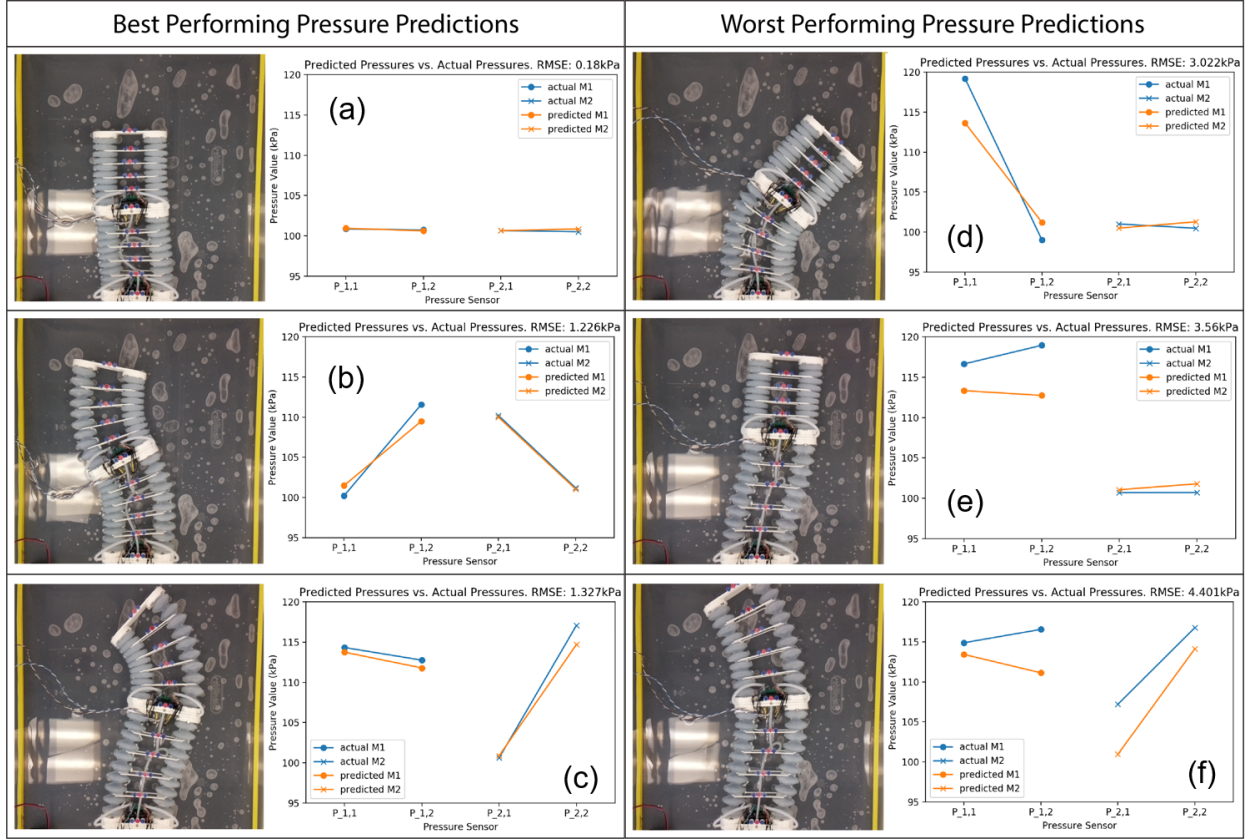


Figure 10: (a-c) Poor performing pressure estimations generated by the backward model. (d-f) Good performing pressure estimations generated by the backward model.

configurable and can be used in a desktop environment. It has been shown that the electronics and fluid networks in the robot are designed so that segments can be added or removed to form a desired robot size. Also, the mounting method used to attach the soft actuators allows for swapping of different types of actuators which may vary in size, shape, and material characteristics. This also allows an actuator to be easily maintained or replaced if one begins to leak or degrades over time. In addition, this robot arm can also be used to develop machine learning models for itself.

With these models performing well, what remains to be tested is their usefulness in the design of a controller for the underwater soft robotic arm. The forward model can be useful in predicting future states over a time horizon in a model predictive controller (MPC), or for generating estimated trajectories in the offline training of a reinforcement learning model. The backward model can provide target pressure values needed for the robot to reach a specified shape. Additionally, it can be used as a sanity check against control inputs that are generated by an MPC. It is predicted that adding a sequence of previous robot shapes as inputs to the backward model would improve its performance. However, in practice these would be difficult to generate offline without also using the forward model.

Some of the robot's current limitations motivate upgrades to the design as future work. Now, its motions are relatively slow because the pump used is small. A more powerful pump would be an interesting addition but would come at the cost of more power draw and a bulkier footprint. Also, adding another actuator to the design of each module could make the robot capable of movement in 3D space instead of being limited to 2D as it is now. Similarly, adding a third module to the existing planar setup would make the robot's shape more complex and the control algorithms more difficult to design. As mentioned in the previous section, it would also be worth experimenting with varying stiffness of the actuators on module 1. Also, a possible research direction is calculating the optimal actuator size and shape given a set of desired motion parameters. Finally, mounting the arm on an underwater ROV and using it at depth would be the ultimate test of its versatility.

There are also exciting research directions that can build on the work presented in this thesis. Various reinforcement learning control algorithms could be developed using the learned model, as well as model predictive controllers to see which performs better under certain conditions. A gripper could be attached to the end of the robot and the model

would need to be adapted to handle changes in mass. The increase the difficulty, the shape of the environment could be changed so that the robot needs to move an object around objects to a target location.

## References

- [1] Aslam Pervez and Jeha Ryu. Safe physical human robot interaction-past, present and future. *Journal of Mechanical Science and Technology*, 22(3):469, 2008.
- [2] Clint Heyer. Human-Robot Interaction and Future Industrial Robotics Applications. *2010 IEEE/RSJ International Conference on Intelligent Robots and Systems*, pages 4749–4754, 2010.
- [3] Pinar Boyraz, Gundula Runge, and Annika Raatz. An Overview of Novel Actuators for Soft Robotics. *Actuators*, 7(3):48, 2018.
- [4] Mark Runciman, Ara Darzi, and George P. Mylonas. Soft Robotics in Minimally Invasive Surgery. *Soft Robotics*, 6(4):423–443, 2019.
- [5] Kevin C. Galloway, Kaitlyn P. Becker, Brennan Phillips, Jordan Kirby, Stephen Licht, Dan Tchernov, Robert J. Wood, and David F. Gruber. Soft Robotic Grippers for Biological Sampling on Deep Reefs. *Soft Robotics*, 3(1):23–33, 2016.
- [6] Andrew D. Marchese, Cagdas D. Onal, and Daniela Rus. Autonomous Soft Robotic Fish Capable of Escape Maneuvers Using Fluidic Elastomer Actuators. *Soft Robotics*, 1(1):75–87, 2014.
- [7] Zhong Shen, Junhan Na, and Zheng Wang. A Biomimetic Underwater Soft Robot Inspired by Cephalopod Mollusc. *IEEE Robotics and Automation Letters*, 2(4):2217–2223, 2017.
- [8] Qi Shen, Zakai Olsen, Tyler Stalbaum, Sarah Trabia, Jameson Lee, Robert Hunt, Kwang Kim, Jaehwan Kim, and Il-Kwon Oh. Basic design of a biomimetic underwater soft robot with switchable swimming modes and programmable artificial muscles. *Smart Materials and Structures*, 29(3):035038, 2020.
- [9] Jun Shintake, Vito Cacucciolo, Herbert Shea, and Dario Floreano. Soft Biomimetic Fish Robot Made of Dielectric Elastomer Actuators. *Soft Robotics*, 5(4):466–474, 2018.
- [10] Hui Feng, Yi Sun, Peter A. Todd, and Heow Pueh Lee. Body Wave Generation for Anguilliform Locomotion Using a Fiber-Reinforced Soft Fluidic Elastomer Actuator Array Toward the Development of the Eel-Inspired Underwater Soft Robot. *Soft Robotics*, 7(2):233–250, 2020.
- [11] Michael Krieg, Isaac Sledge, and Kamran Mohseni. Design considerations for an underwater soft-robot inspired from marine invertebrates. *Bioinspiration & Biomimetics*, 10(6):065004, 2015.
- [12] F Giorgio-Serchi, A Arienti, F Corucci, M Giorelli, and C Laschi. Hybrid parameter identification of a multi-modal underwater soft robot. *Bioinspiration & Biomimetics*, 12(2):025007, 2017.
- [13] Guorui Li, Xiangping Chen, Fanghao Zhou, Yiming Liang, Youhua Xiao, Xunuo Cao, Zhen Zhang, Mingqi Zhang, Baosheng Wu, Shunyu Yin, Yi Xu, Hongbo Fan, Zheng Chen, Wei Song, Wenjing Yang, Binbin Pan, Jiaoyi Hou, Weifeng Zou, Shunping He, Xuxu Yang, Guoyong Mao, Zheng Jia, Haoifei Zhou, Tiefeng Li, Shaoxing Qu, Zhongbin Xu, Zhilong Huang, Yingwu Luo, Tao Xie, Jason Gu, Shiqiang Zhu, and Wei Yang. Self-powered soft robot in the Mariana Trench. *Nature*, 591(7848):66–71, 2021.
- [14] Jie Han, Weitao Jiang, Hongjian Zhang, Biao Lei, Lanlan Wang, and Hongzhong Liu. Submersible Soft-Robotic Platform for Noise-Free Hovering Utilizing Liquid–Vapor Phase Transition. *Advanced Intelligent Systems*, 3(1):2000147, 2021.
- [15] Zheyuan Gong, Jiahui Cheng, Xingyu Chen, Wenguang Sun, Xi Fang, Kainan Hu, Zhixin Xie, Tianmiao Wang, and Li Wen. A Bio-inspired Soft Robotic Arm: Kinematic Modeling and Hydrodynamic Experiments. *Journal of Bionic Engineering*, 15(2):204–219, 2018.
- [16] Shunichi Kurumaya, Brennan T. Phillips, Kaitlyn P. Becker, Michelle H. Rosen, David F. Gruber, Kevin C. Galloway, Koichi Suzumori, and Robert J. Wood. A Modular Soft Robotic Wrist for Underwater Manipulation. *Soft Robotics*, 5(4):399–409, 2018.
- [17] Nina R. Sinatra. Ultrgentle manipulation of delicate structures using a soft robotic gripper. *Science Robotics*, 8 2019.
- [18] Zheyuan Gong, Jiahui Cheng, Kainan Hu, Tianmiao Wang, and Li Wen. An Inverse Kinematics Method of a Soft Robotic Arm with Three-Dimensional Locomotion for Underwater Manipulation. *2018 IEEE International Conference on Soft Robotics (RoboSoft)*, pages 516–521, 2018.

- [19] Zhong Shen, Hua Zhong, Erchao Xu, Runzhi Zhang, Ki Chun Yip, Lawrence Long Chan, Leo Lai Chan, Jia Pan, Wenping Wang, and Zheng Wang. An Underwater Robotic Manipulator with Soft Bladders and Compact Depth-Independent Actuation. *Soft Robotics*, 7(5):535–549, 2020.
- [20] Jamie Luong, Paul Glick, Aaron Ong, Maya S. deVries, Stuart Sandin, Elliot W. Hawkes, and Michael T. Tolley. Eversion and Retraction of a Soft Robot Towards the Exploration of Coral Reefs. *2019 2nd IEEE International Conference on Soft Robotics (RoboSoft)*, 00:801–807, 2019.
- [21] Robert Bogue. Underwater robots: a review of technologies and applications. *Industrial Robot: An International Journal*, 42(3):186–191, 2015.
- [22] Fan Xu, Hesheng Wang, Kwok Wai Samuel Au, Weidong Chen, and Yanzi Miao. Underwater Dynamic Modeling for a Cable-Driven Soft Robot Arm. *IEEE/ASME Transactions on Mechatronics*, 23(6):2726–2738, 2018.
- [23] Tao Du, Josie Hughes, Sebastien Wah, Wojciech Matusik, and Daniela Rus. Underwater Soft Robot Modeling and Control With Differentiable Simulation. *IEEE Robotics and Automation Letters*, 6(3):4994–5001, 2020.
- [24] Robert J. Webster and Bryan A. Jones. Design and Kinematic Modeling of Constant Curvature Continuum Robots: A Review. *The International Journal of Robotics Research*, 29(13):1661–1683, 2010.
- [25] G. Runge, M. Wiese, L. Gunther, and A. Raatz. A framework for the kinematic modeling of soft material robots combining finite element analysis and piecewise constant curvature kinematics. *2017 3rd International Conference on Control, Automation and Robotics (ICCAR)*, pages 7–14, 2017.
- [26] Kevin Wandke and Y Z. MOOSE-Based Finite Element Hyperelastic Modeling for Soft Robot Simulations. *IEEE Access*, 9:139627–139635, 2021.
- [27] Thomas George Thuruthel, Benjamin Shih, Cecilia Laschi, and Michael Thomas Tolley. Soft robot perception using embedded soft sensors and recurrent neural networks. *Science Robotics*, 4(26):eaav1488, 2019.
- [28] Jaewoong Jung, Myungsun Park, DongWook Kim, and Yong-Lae Park. Optically Sensorized Elastomer Air Chamber for Proprioceptive Sensing of Soft Pneumatic Actuators. *IEEE Robotics and Automation Letters*, 5(2):2333–2340, 2019.
- [29] Keene Chin, Tess Hellebrekers, and Carmel Majidi. Machine Learning for Soft Robotic Sensing and Control. *Advanced Intelligent Systems*, 2(6):1900171, 2020.
- [30] Matthias Rolf and Jochen J. Steil. Efficient Exploratory Learning of Inverse Kinematics on a Bionic Elephant Trunk. *IEEE Transactions on Neural Networks and Learning Systems*, 25(6):1147–1160, 2014.
- [31] Morgan T. Gillespie, Charles M. Best, Eric C. Townsend, David Wingate, and Marc D. Killpack. Learning Nonlinear Dynamic Models of Soft Robots for Model Predictive Control with Neural Networks. *2018 IEEE International Conference on Soft Robotics (RoboSoft)*, pages 39–45, 2018.
- [32] Phillip Hyatt, David Wingate, and Marc D. Killpack. Model-Based Control of Soft Actuators Using Learned Non-linear Discrete-Time Models. *Frontiers in Robotics and AI*, 6:22, 2019.
- [33] Thomas George Thuruthel, Egidio Falotico, Federico Renda, and Cecilia Laschi. Learning dynamic models for open loop predictive control of soft robotic manipulators. *Bioinspiration & Biomimetics*, 12(6):066003, 2017.
- [34] Xuanke You, Yixiao Zhang, Xiaotong Chen, Xinghua Liu, Zhanchi Wang, Hao Jiang, and Xiaoping Chen. Model-Free Control for Soft Manipulators Based on Reinforcement Learning. *2017 IEEE/RSJ International Conference on Intelligent Robots and Systems (IROS)*, pages 2909–2915, 2017.
- [35] Ge Fang, Xiaomei Wang, Kui Wang, Kit-Hang Lee, Justin D. L. Ho, Hing-Choi Fu, Denny Kin Chung Fu, and Ka-Wai Kwok. Vision-Based Online Learning Kinematic Control for Soft Robots Using Local Gaussian Process Regression. *IEEE Robotics and Automation Letters*, 4(2):1194–1201, 2019.